applied optics

Patterned liquid crystal polymer C-plate retarder and color polarizer

Sawyer Miller,* Linan Jiang, Xingzhou Tu, and Stanley Pau

James C. Wyant College of Optical Sciences, University of Arizona, 1630 East University Boulevard, Tucson, Arizona 85721, USA
**Corresponding author: samiller@optics.arizona.edu*

Received 16 December 2020; revised 19 January 2021; accepted 21 January 2021; posted 22 January 2021 (Doc. ID 416845); published 12 February 2021

The patternability and guest–host interaction with dichroic dye and C-plate liquid crystal polymer (LCP) materials are investigated, and the optical properties of a thin film C-plate retarder and polarizer are studied and compared with theory. The C-plate retarder is a waveplate made of a uniaxial LCP where the optical axis of the LCP is parallel to the surface normal of the optic. No retardance is observed at a normal angle of incidence and retardance grows as the angle of incidence increases. The C-plate polarizer is a C-plate retarder with LCP as the host and a dichroic dye as the guest. The linear diattenuation (LD) of the linear polarizer is zero at a normal angle of incidence and grows with an increasing angle of incidence. Both the C-plate retarder and polarizer can be patterned with minimum feature size down to 2 μm by using ultraviolet photolithography and plasma etching. A planarization process is also developed to deposit a cover layer on top of the pattern to reduce optical loss and to serve as a barrier for subsequent layers.

https://doi.org/10.1364/AO.416845

1. INTRODUCTION

Thin film retarders and polarizers are essential optical components in many different applications ranging from polarimetry [1–6], interferometry [7,8], and display technologies [9–19]. The most common type of retarder is made from a uniaxial birefringent crystal with the optical axis of the crystal in the direction perpendicular to the surface normal of the optic. This configuration is known as an A-plate [1,20,21]. Combinations of A-plates are commonly used in LCD and LED displays to control glare from ambient lighting by generating images with high contrast ratios [13–16,22,23]. However, A-plates have a retardance that changes as a function of the angle and field of view. The actual retardance map has an astigmatic saddle contour [1,20,21], resulting in an ineffective antiglare filter at angles of higher incidence.

To help combat this issue, many researchers have turned to biaxial materials [14] and other uniaxial materials in different configurations apart from the A-plate [13,15,16,22]. The most notable of these configurations is the C-plate, where the optical axis of a uniaxial material is parallel to the surface normal of the optic [1,20,21]. Many different designs have been suggested using different configurations: positive A-plates, where the extraordinary index of refraction is greater than the normal index of refraction; negative A-plates, where the extraordinary index of refraction is less than the ordinary index of refraction; and C-plates to generate retarders that have a nearly constant retardance value across the entire field of view. In some cases, these retarders have fields of view of upward of 80 deg [13,16].

Liquid crystal polymer (LCP) in the nematic phase is an example of some of the uniaxial materials used to fabricate retarders. The ease of fine-tuning the material properties, such as the retardance magnitude and alignment orientation, makes LCP a versatile material for thin film retarders and polarizers [24]. LCP can also be patterned using photolithography techniques, with spatial resolution down to sub-10 micron feature sizes [4,24]. Features such as these are used on filters for imaging polarimeters and displays. The LCP can also participate in the guest–host interaction, where a dichroic dye is added to the LCP and aligned within the liquid crystal matrix to produce a polarizer [25–29].

In this work, we demonstrate the fabrication and patterning of C-plate LCP material. The ability of the C-plate material to participate in the guest-host interaction is also demonstrated, as we add a dichroic dye to the LCP and fabricate a C-plate polarizer with no linear diattenuation (LD) at normal incidence and an increasing LD as the angle of incidence increases. The nonuniform chromatic response of the dye determines the polarizer color. A detailed description is provided in Appendix A. Other optical components exhibiting similar behavior include the pile-of-plates polarizer, which uses many index of refraction interfaces and Fresnel reflections. The C-plate retarder has been used in numerous designs to produce retarders with wide fields of view. However, with the addition of dichroic dye, the C-plate polarizer enables a high-performance wide field-of-view polarization control with fewer layers. The optical properties of the C-plate retarder and polarizer are measured and compared with

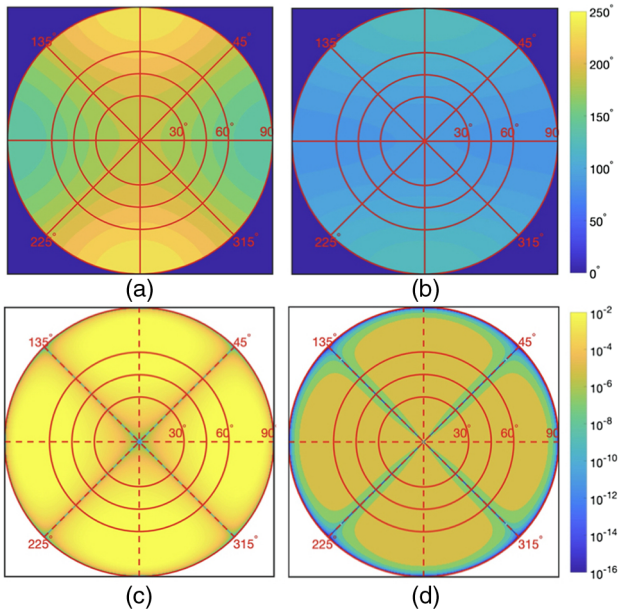

Fig. 1. (a) Retardance contour map of EMD RMM141C at 550 nm. Notice the apparent astigmatic saddle contour. (b) Retardance contour map of a positive A-plate, negative A-plate, and positive C-plate stack following [16] at 550 nm. The retardance over the entire field of view is greatly improved. (c) Contour map of the log of the amount of transmitted light through ideal crossed polarizers at 470 nm. Up to 3% light is transmitted, even with ideal polarizers. Notice the areas of highest linear diattenuation are along the crossed transmission axes at ±45°. This can be viewed with blue coloring on the simulation. (d) Contour map of the C-plate polarizer and negative C-plate inserted between crossed polarized. The amount of transmitted light is reduced by a factor of 94, nearly two orders of magnitude across the entire viewing cone of ±90°. Both (c) and (d) are represented in log-scale of transmittance, which ranges from negative infinity to zero.

theoretical calculations. The material can be patterned with a minimum spatial resolution of 2 μm.

2. THEORY

Both the C-plate retarder and polarizer are important and effective components in the construction of polarization-sensitive optical systems with wide fields of view. The C-plate retarder has been extensively used in antiglare filters [13,14,16] used by LCD and LED displays to improve the contrast ratios of these displays and to reduce lateral color shift [19]. In most of the antiglare filters used, a wide field of view quarter-wave plate is needed [13,14,16]. Figure 1(a) shows a simulation of an A-plate over a field of view of ±90°. The characteristics are that of an A-plate made of a 2 micron thick LCP (RMM141C, EMD Performance Materials) designed for a wavelength of 550 nm. A notable feature is the large variation in the astigmatic retardance map as a function of the field of view. Figure 1(b) shows improvement of the retardance across the field of view when a positive A-plate is combined with a negative A-plate and a positive C-plate [16]. The retardance across the field of view deviates much less and a wide field of view quarter-wave plate is achieved. Figures 1(a) and 1(b) are calculated using Eq. (2). In Fig. 1(c) two ideal crossed polarizers are shown as a function of the field of view at 470 nm. Slight light leakage is shown and the expected Maltese cross pattern is observed. To reduce the amount of light leakage, a C-plate polarizer and negative C-plate are inserted between the ideal crossed polarizers. The negative C-plate has the same retardance magnitude as the C-plate polarizer host material. The amount of light leakage is reduced by a factor of 94, as shown in Fig. 1(d). Figures 1(c) and 1(d) are calculated using the extended Jones matrix method [20,21]. Table 1 compares the performance of the current design with published works. The transmittance between crossed polarizers is shown as well as the angle of the viewing cone over which the design is valid. Our design with only two layers, a C-plate polarizer and a negative C-plate retarder, performs as well as existing designs over the operating wavelengths of the dichroic dye.

Table 1. Comparison of Viewing Cone Angle and Minimum Transmittance for Different Designs[a]

References	Viewing Cone	Number of Layers	Layer Configuration (Top to Bottom)	Minimum Transmittance
Ref. [13]	±80°	5	Biaxial plate, +A, −C, MVA cell, +A	5×10^{-4}
Ref. [14]	±85°	2	Biaxial plate, Biaxial plate	8.23×10^{-5}
Ref. [15]	±85°	10	+A, +C, +A, −C, +A, +A, −C, +A, +C, +A	3.79×10^{-4}
Ref. [16]	±90°	3	+A, −A, +C	2.87×10^{-4}
This work	±90°	2	C-plate polarizer, -C	4.31×10^{-4}

[a]±A denotes a positive or negative A-plate, respectively. ±C denotes a positive or negative C-plate, respectively.

A. C-plate Retarder

The retardance of a general uniaxial medium, γ, is computed as

$$\gamma = (k_{e,z} - k_{o,z})d, \tag{1}$$

where d is the thickness of the film, and $k_{e,z}$ and $k_{o,z}$ are the extraordinary and ordinary components of the $\vec{k}$-vector traveling through the uniaxial medium. $k_{e,z}$ and $k_{o,z}$ are characterized by: n_e, the extraordinary index of refraction; n_o, the ordinary index of refraction; d, the thickness of the film; and the optical axis orientation defined by a polar angle, θ_n, and an azimuthal angle, ϕ_n. The characteristics of the incident light must also be considered, including: the wavelength of incident light λ, the angle of incidence described by a polar angle, θ_0, and an azimuthal angle, ϕ_0. These parameters are consolidated into two equations given by [20,30]

$$k_{e,z} = \frac{2\pi}{\lambda}\left[\frac{n_e n_o}{\epsilon_{zz}}\sqrt{\epsilon_{zz} - \left(1 - \frac{n_e^2 - n_o^2}{n_e^2}\cos^2\theta_n \sin^2(\phi_n - \phi_o)\right)\sin^2\theta_0} - \frac{\epsilon_{xz}}{\epsilon_{zz}}\sin\theta_0\right], \tag{2}$$

$$k_{o,z} = \frac{2\pi}{\lambda}\sqrt{n_o^2 - \sin^2\theta_0}, \tag{3}$$

where $\epsilon_{xz} = (n_e^2 - n_o^2)\sin\theta_n\cos\theta_n\cos(\phi_n - \phi_o)$ and $\epsilon_{zz} = n_o^2 + (n_e^2 - n_o^2)\sin^2\theta_n$. Due to the orientation of the LCP molecule, the retardance of the C-plate is only dependent on the polar component, θ_0, of the angle of incidence from the incoming light. No azimuthal considerations must be made in the calculation.

A comparison between an A-plate, where the optical axis (OA) is perpendicular to the surface normal of the optic, $\hat{n}$, is shown at the top of Fig. 2(a). Comparatively, a C-plate configuration is shown at the bottom of Fig. 2(a), where the OA is parallel to the $\hat{n}$ of the optic. The index ellipsoid of a C-plate is shown in Fig. 2(b). The angular dependencies of the LCP are better visualized using the index ellipsoid depiction. Notice as the polar component, θ_0, of the angle of incidence of the $\vec{k}$-vector increases, the projection onto n_e also increases. The linear retardance and LD increase with the angle of incidence as a result.

B. C-plate Polarizer

Properties of the C-plate polarizer can be described using Eqs. (2) and (3), and inserting them into a Jones matrix [1,20,30],

$$J = \begin{bmatrix} e^{-ik_{e,z}d} & 0 \\ 0 & e^{-ik_{o,z}d} \end{bmatrix}. \tag{4}$$

It is important to note that the indices of refraction become complex when the dichroic dye is added to the LCP in this sample. The quantities described by Eqs. (2) and (3) become complex and all polarizing properties of the LCP with dye can be calculated. Prior knowledge of the thickness of the layer d is needed to fully characterize the film. The component values for $\vec{k}$ are then plugged into Eq. (4) and a Jones matrix can be generated for every angle of incidence. These Jones matrices are then subsequently transformed into Mueller matrices for further analysis in

$$M = \frac{1}{2}\begin{bmatrix} |e^{-ik_{e,z}d}|^2 + |e^{-ik_{o,z}d}|^2 & |e^{-ik_{e,z}d}|^2 - |e^{-ik_{o,z}d}|^2 & 0 & 0 \\ |e^{-ik_{e,z}d}|^2 - |e^{-ik_{o,z}d}|^2 & |e^{-ik_{e,z}d}|^2 + |e^{-ik_{o,z}d}|^2 & 0 & 0 \\ 0 & 0 & e^{-d\nu_1}\cos(d\nu_2) & e^{-d\nu_1}\sin(d\nu_2) \\ 0 & 0 & -e^{-d\nu_1}\sin(d\nu_2) & e^{-d\nu_1}\cos(d\nu_2) \end{bmatrix}, \tag{5}$$

where $\nu_1 = \mathrm{Im}(k_{e,z}) + \mathrm{Im}(k_{o,z})$ and $\nu_2 = \mathrm{Re}(k_{e,z}) - \mathrm{Re}(k_{o,z})$. LD values are then calculated using the generated Mueller matrices in Eq. (5) as a function of the incident angle, as shown in

$$\mathrm{LD}(\theta) = \frac{\sqrt{m_{0,1}^2(\theta) + m_{0,2}^2(\theta)}}{m_{0,0}(\theta)}, \quad 0 \le \mathrm{LD} \le 1, \tag{6}$$

where the matrix indices are consistent with Chipman [1].

LD describes the strength of a polarizing element, where LD varies from 1 for an ideal polarizer to 0 for an element that transmits all polarization states equally [1]. Finally, n_e and n_o are determined using the calculated Mueller matrix values. An extreme value of a 90° angle of incidence would correspond to a traditional LCP polarizer where the dichroic dye is suspended in an A-plate nematic LCP matrix [25,27,28].

At lower angles of incidence, light transmitted through the C-plate polarizer experiences retardance. To effectively use the C-plate polarizer between crossed linear polarizers, an additional negative C-plate layer is added. Equal but opposite retardance is needed in the negative C-plate to counteract the C-plate polarizer, allowing for the crossed linear polarizers to achieve high LD across all angles of incidence.

Eigenpolarization analysis was also performed to verify that the films were operating correctly. Polarization optics with Mueller matrices in the form of Eq. (5) will always have eigenpolarizations of $[1, 1, 0, 0]^T$ and $[1, -1, 0, 0]^T$ [31]. Theoretical

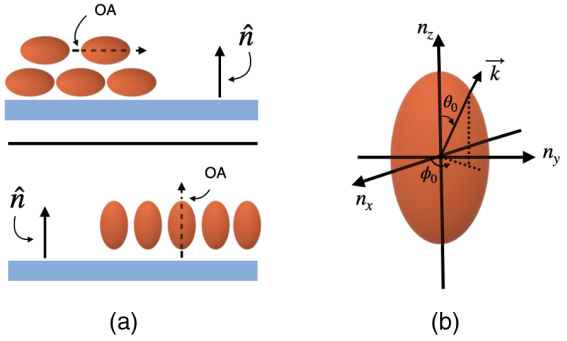

Fig. 2. (a) A comparison of OA alignment and $\hat{n}$ of the optic between an A-plate (top) and C-plate (bottom). (b) An index ellipsoid depicting the orientation of the LCP molecule and corresponding incident light's $\vec{k}$-vector. The optical axis of the molecule is oriented parallel to the surface normal of the substrate.

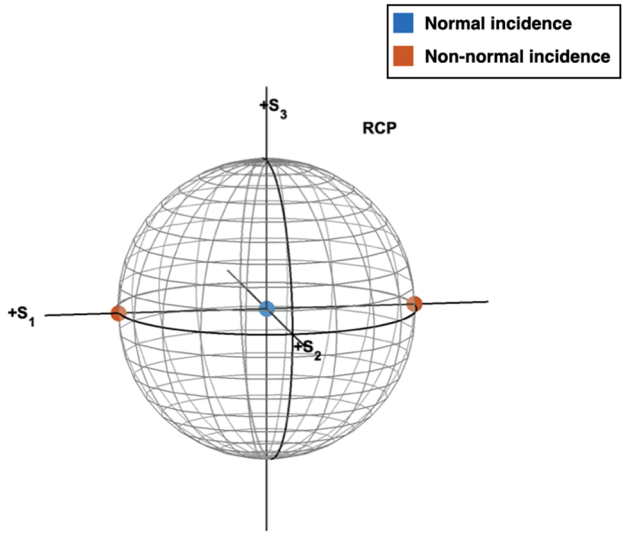

Fig. 3. Theoretical eigenpolarizations plot on the Poincaré sphere as a function of angle of incidence for the C-plate retarder and polarizer. All eigenpolarizations lie on the S_1 axis in agreement with the Mueller matrix in Eq. (5). One state is at the origin, representative of unpolarized light. This is the eigenpolarization of the C-plate retarder and polarizer at normal incidence, where no polarization properties are observed.

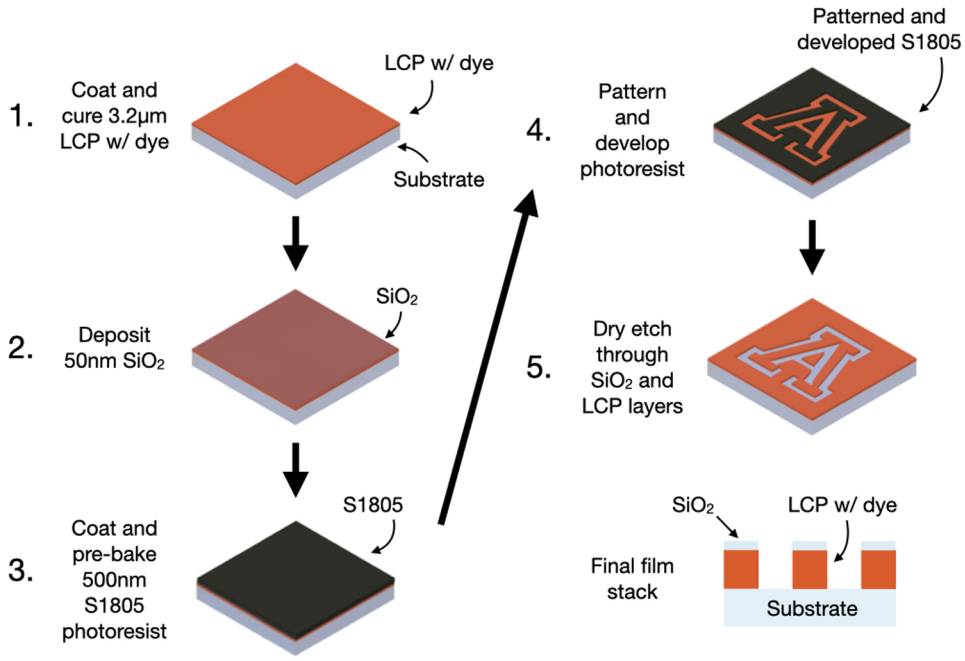

Fig. 4. Fabrication and patterning process for the C-plate polarizer. The only difference in fabrication of the C-plate retarder is the absence of the dye in the LCP solution. A final thin-film schematic is shown in the bottom right corner.

eigenpolarizations of the C-plate retarder and polarizer are plotted in Fig. 3 on the Poincaré sphere as a function of angle of incidence. All points lie on the S_1 axis. The point at the origin is representative of unpolarized light and is the eigenpolarization of the identity matrix, equal to that of Eq. (5) at normal incidence.

3. EXPERIMENTAL METHODS AND MATERIALS

A. Materials and Characterization

All materials used in this study are commercially available and do not require further purification. The C-plate LCP material is model RMM1704 (EMD Performance Materials, a unit of Merck KGaA, Darmstadt, Germany). The LCP is added to a 50/50 volume concentration of toluene and acetone at 40% weight ratio. The dichroic dye (model Orange AZO 1, Nematel GmbH & Co. KG, Mainz, Germany) is added to the solvent solution at 25 mg/mL. The entire solution is then gently agitated until completely homogeneous. The substrates used are made from soda-lime glass. All samples are measured with a Mueller matrix polarimeter (Axometrics, Huntsville, AL, USA). The thickness of the film is measured using surface profilometer (Dektak 150, Veeco, Plainville, NY, USA).

B. Fabrication Process

Both the C-plate retarder and C-plate polarizer with added dye are fabricated in the same process, with the only difference being the solution dispensed on the wafer in Step 2 below. The fabrication process for the samples has seven steps:

1. The wafer is cleaned and prepared using an oxygen plasma treatment for 1 min.
2. The LCP material is dispensed through a 0.2 μm PTFE filter onto the substrate and spin-coated at 1000 RPM for 30 s, as shown in Fig. 4, Step 1. The substrate is then baked at 65 °C for 1 min.
3. The wafer is then exposed to 150 mJ/cm^2 at 365 nm under a nitrogen atmosphere to cure the LCP.
4. 50 nm of SiO_2 is evaporated onto the sample using a Temescal FC2500, as shown in Fig. 4 Step 2.
5. A 500 nm thick layer of Microposit S1805 photoresist is spin-coated onto the sample and prebaked as shown in Fig. 4, Step 3.
6. The photoresist is exposed using a Heidelberg MLA150 maskless aligner with a computer designed pattern and a dosage of 54 mJ. The photoresist is then developed using Microposit MF319 shown in Fig. 4, Step 4. Several different patterns were used throughout the study. Section 4 details two of these patterns. These test patterns allowed us to determine the resolution limit and pattern fidelity of the patterning process.
7. The patterned sample is then etched in two steps with a Plasmatherm DSE III using deep reactive ion etching techniques. First a SiO_2 etch using O_2 and CHF_3 is completed and the LCP is exposed under the developed resist. Then a polymer etch using O_2 and Ar is performed until completion using the remaining SiO_2 as a hard mask. The remaining undeveloped photoresist is also etched away during this process. Complete plasma etching parameters are given in Table 2. The completed sample is shown in Fig. 4, Step 5.

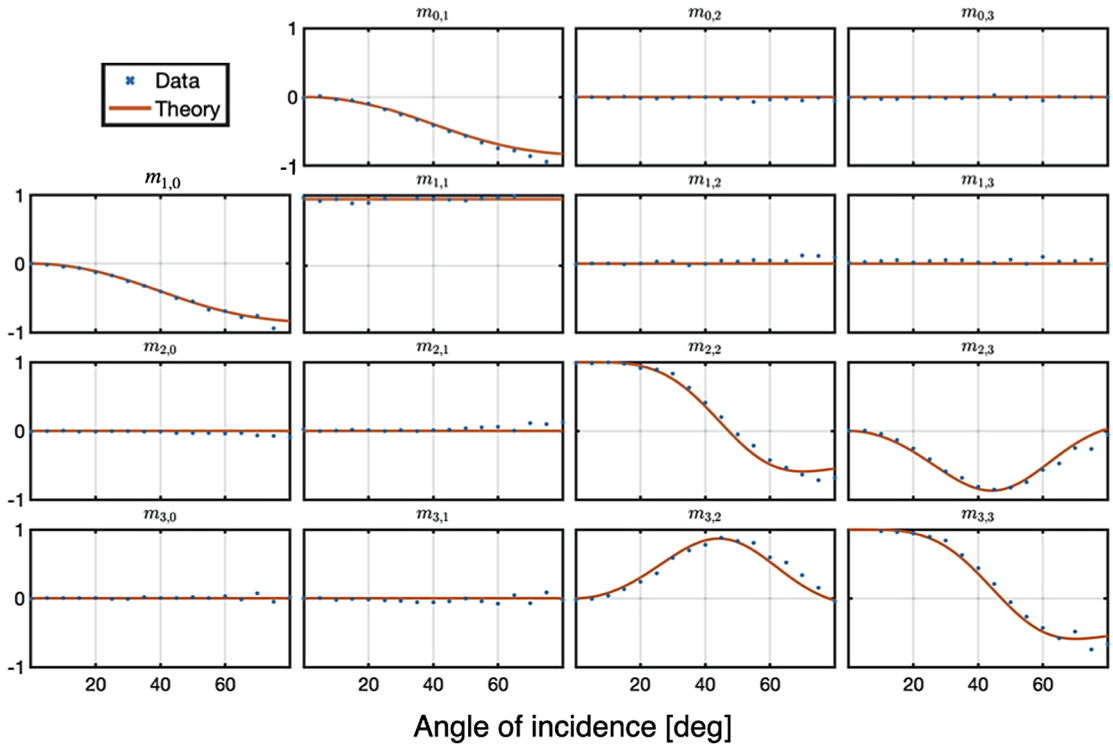

Fig. 5. Theoretical and measured normalized Mueller matrices as a function of angle for the C-plate polarizer taken at 470 nm. The LD and linear polarizance follow the same pattern, showing this film is effective as a polarizer and an analyzer.

Table 2. Plasma Etching Parameters Used in the Fabrication of the C-plate Polarizer

Material	Gas Flow Rate	Pressure	ICP Power	RIE Power	Etch Time
SiO_2	CHF_3: 50 sccm O_2: 5 sccm	5 mT	400 W	100 W	75 s
LCP	O_2: 50 sccm Ar: 5 sccm	5 mT	500 W	59 W	345 s

4. RESULTS

By using Eqs. (2)–(6) to fit the calculated LD to the measured LD as a function of angle of incidence, the indices of refraction can be determined for the C-plate polarizer. The parameters of the film were found to be $n_e = 1.65 - 0.085i$ and $n_o = 1.5 - 0.011i$ at 470 nm, the wavelength of highest diattenuation. Further characterization of the dichroic dye as a function of wavelength is provided in Appendix A. It should be noted that a dichroic dye of a different color can be added to the C-plate. For broadband operation, a mixture of dichroic dyes can be used in place of the current orange dichroic dye. The thickness d was measured to be 3.2 μm. The measured normalized Mueller matrix at 470 nm of the completed C-plate polarizer is shown as function of the angle of incidence in Fig. 5. Simulated, normalized Mueller matrix data using Eq. (5) is plotted alongside, showing a good fit across all angles of incidence. The transmission of the C-plate polarizer film without a substrate at normal incidence measured at 470 nm was found to be 53%.

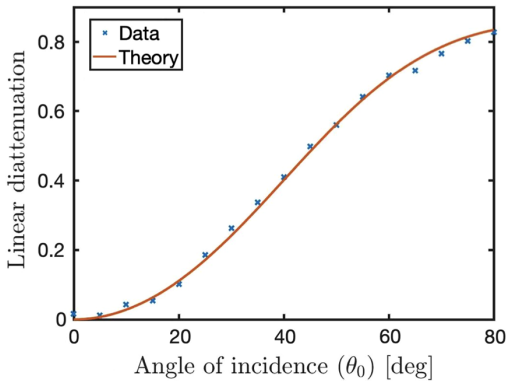

Fig. 6. Theoretical and measured LD of a C-plate polarizer as a function of angle of incidence at 470 nm. The parameters of the simulation include n_o, n_e, λ of the incident light, and d of the film. Fresnel reflection effects from the substrate are eliminated in the data measurement.

The LD properties are clearly seen as increasing in magnitude as a function of the increasing angle in element $m_{0,1}$. Theoretical LD values fit well with the measured LD values, as shown in Fig. 6.

The linear polarizance increases in magnitude in the same manner in element $m_{1,0}$. Therefore, this film is homogeneous and equally effective as a polarizer and as an analyzer. Other polarizing properties are included in the retarder 3×3 submatrix. Elements $m_{2,2}$, $m_{2,3}$, $m_{3,2}$, and $m_{3,3}$ start at low angles of incidence with no polarizing properties. As the angle of incidence increases, the 3×3 submatrix parameters increase or decrease, deviating from the identity matrix and demonstrating

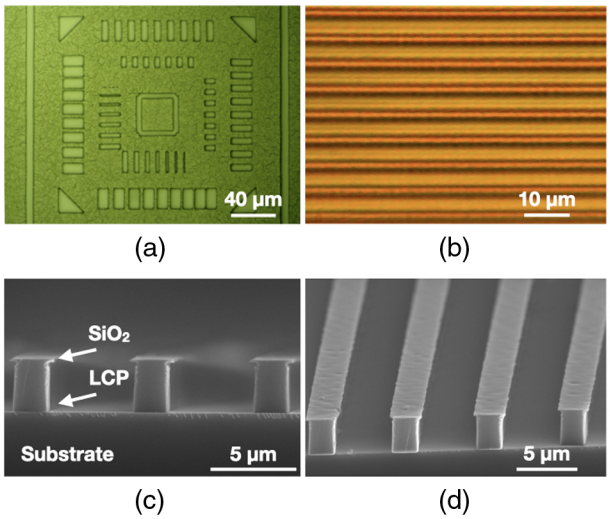

Fig. 7. (a) Microscope image of the patterned C-plate polarizer after etching. (b) Microscope image of patterned C-plate polarizer sample after etching with bar pattern. (c) SEM image of a cross section in a completed C-plate polarizer sample. The resolution of the patterning is determined to be 2 μm. (d) SEM image with an elevated view showing more detail of the patterned sample.

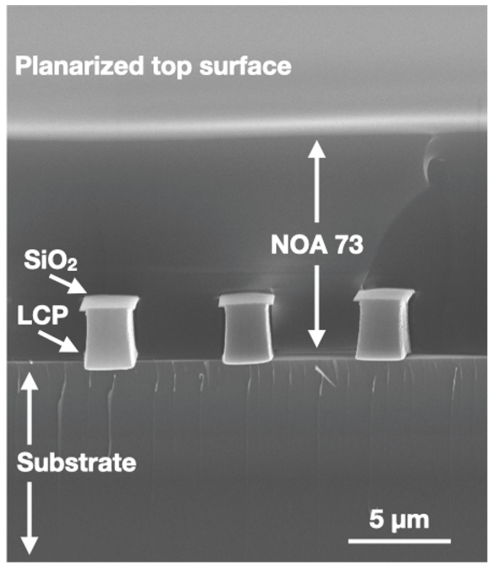

Fig. 8. SEM cross-section of the patterned LCP with NOA 73 applied. The NOA 73 is measured to be 10.9 μm in thickness. The SiO_2 hard mask and patterned LCP are visible, as well as the substrate.

linear retardance properties. As expected, other parameters describing circular diattenuation or circular polarizance are zero throughout the measurement of the film. Circular retardance measurements also are near zero. It is important to note that the polarizing Fresnel reflection and transmission coefficients of the substrate are considered in this data measurement, and only the C-plate polarizer film is described in Fig. 5. The Fresnel coefficients of the substrate were accounted for by measuring a blank substrate with the Axometrics Mueller matrix polarimeter. The measured Mueller matrix of the substrate was then inverted and multiplied by the measured LCP and the dye sample Mueller matrix. The resultant matrix is only that of the film.

The patterning resolution of the C-plate is studied using a microscope. Figure 7(a) shows a patterned C-plate polarizer sample after plasma etching. The resolution of the process is determined by the smallest patterned feature resolvable. In this case, we determined the resolution to be about 2 μm. Other samples were patterned using bar features 2 μm thick with 5 μm in between bars. Figure 7(b) shows a microscope image of the patterned C-plate polarizer with bar pattern after etching. Figure 7(c) shows an SEM image of the cross section of the patterned sample. Detailed in the image are the locations of the remaining SiO_2 hard mask, the patterned LCP, and the substrate. An elevated view of the etched sample is shown in Fig. 7(d).

The effect of patterning is also studied with the Axometrics Mueller matrix polarimeter to investigate how the polarization proprieties change from bulk film to a finalized patterned sample. It should be noted that testing of the film's performance was undertaken on a sample that experienced the entire patterning process, but was tested in locations where unpatterned, bulk film remained. This was done to ensure any polarization measurements were not affected by diffraction. The LD of the film before and after is calculated to have a small difference of 5% at 80° angle of incidence. The complete process does cause some loss of LD, and this can be attributed to the etch process. Calculation shows that a loss of about 100 nm of LCP can occur in the observed lower LD values. Small amounts of dye bleaching during plasma etching could also cause the lower diattenuation values. All other parameters remain the same. Notably the depolarization index stays constant, at a value of one, implying very little scattering is occurring as light travels through the sample [32].

The use of plasma etching gives the ability to produce features with sharp edges and rapid changes in refractive index. These properties can lead to a sample that is highly scattering and diffractive, both of which are undesirable for a polarization optic. Furthermore, for a fabrication process involving multiple layers of LCP, the topography left by the patterning makes coating of a subsequent layer difficult. To mitigate this problem, application of an isotropic material, with a refractive index close to that of the LCP, is needed to fill the voids created by patterning. The coating leads to a reduction of light scattering by providing a smooth transition of index of refraction between materials and of the diffractive effects by decreasing the optical path difference. The planarization process would also facilitate the uniform coating of multiple stacks of LCP on top of the patterned layer.

To achieve the planarization of the patterned film, Norland optical adhesive (NOA) 73 is applied by spin-coating to the patterned sample. The NOA 73 is spin-coated at 3000 RPM on the patterned LCP sample and then UV cured with 150 mJ/cm^2 at 365 nm in a nitrogen atmosphere. An SEM cross-section of a sample is shown in Fig. 8, showing the uniform filling and flatness of the coating.

The NOA 73 has a refractive index of 1.56 at 589 nm and a viscosity of 130 cps at room temperature [33], resulting in a film thickness of 10.9 μm. Further refinement of the spin speed, as well as plasma etching can reduce the overall film thickness down to the 3.2 μm thickness of the LCP.

It should be noted that the high resolution of the patterning is not an inherent property of the LCP material itself; rather it is a byproduct of using high-resolution lithography instrumentation. However, the fact that the material can be patterned to such resolution where individual pixel sizes are possible should be noted. Traditionally, LCP materials have been patterned with either a rubbed polyimide or a patterned photoalignment material. Such patterning has a finite transition region between LCP aligned in different directions [34]. Patterning by plasma etching eliminates this finite transition region. As the C-plate material does not need an alignment layer, it was a good candidate to experiment with high-resolution lithography, plasma etching, and LCP.

5. CONCLUSION

In this work, C-plate LCP was used to fabricate thin film retarder and polarizer. Both films can be patterned in high resolution using conventional optical lithography and etch. The C-plate retarder is already widely used in LED and LCD displays for antiglare filters and field-of-view compensation filters. The ability to pattern the C-plate retarder material in conjunction with other A-plate material would allow for enhanced polarization analysis filters for use in polarimeters where large numerical apertures can be used and the Stokes parameters can be reconstructed accurately. [3]. The novel C-plate polarizer uses a dichroic dye as a guest in a liquid crystal host. The C-plate polarizer film has a LD as a function of angle of incidence, where increasing the angle of incidence increases the LD. This type of film can be used to reduce the amount of light leakage through crossed polarizers for wide field-of-view applications. The fabricated sample in this work is able to reduce the amount of light leakage through ideal polarizers by a factor of 94. While only one layer of LCP is used in this work, the C-plate material can, in principle, be applied in multiple layers, allowing for thin-film stacks of A-plates, C-plates, and polarizers. Patterning of such devices can be achieved close to the pixel size of the current imaging sensors (i.e., around a micron), thus enabling application in imaging polarimeters and interferometers that can accept high numerical aperture beams for increased resolution. The resolution of the patterning also enables integrated photonic applications. Solutions such as polarizing/polarization maintaining photonic circuits made from the undoped or doped C-plate material would allow for efficient filtering, polarization control, and conversion of signals.

The C-plate polarizer device can be compared to another well-known angular dependent polarizer, the pile-of-plates polarizer. Whereas the pile-of-plates polarizer uses numerous, alternating refractive index interfaces to polarize light, the C-plate polarizer operates by using a single layer thin film. For a pile-of-plates polarizer, the LD curve as a function of the angle of incidence peaks at the Brewster angle and then rapidly decreases as the angle of incidence increases. In contrast, the C-plate polarizer has a continually increasing LD curve as a function of the angle of incidence, as shown in Fig. 6. Moreover, the pile-of-plates polarizer transmits p-polarization while reflecting s-polarization. The C-plate polarizer transmits s-polarization and absorbs p-polarization. Finally, the pile-of-plates polarizer is a pure polarization device. The C-plate polarizer, using the guest–host interaction, is a retarder and a polarizer enabling the simplification of multilayer retarder and polarizer systems into a single LCP layer.

APPENDIX A: DICHROIC DYE PERFORMANCE AS A FUNCTION OF WAVELENGTH

The dichroic dye used in this work provides linear polarization properties in the band of 420–550 nm. Wavelengths outside of this band do not experience high amounts of LD.

As shown in Fig. 9, the LD as a function of wavelength peaks in the region from 470–490 nm. The data was taken using an Axometrics Mueller matrix polarimeter at an angle of incidence of 55°. Polarizing Fresnel reflections and transmissions of the substrate are considered in this calculation and only the polarizing properties of the C-plate polarizing film are displayed. The transmission of the sample is also plotted in Fig. 9. The regions of highest diattenuation also occur near the regions of highest absorption. The LCP can be loaded with more dye, resulting in higher diattenuation values. However, increasing the dye loading generally reduces the transmission of the sample [35].

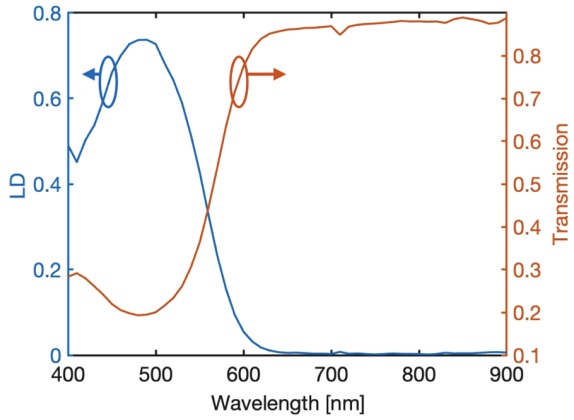

Fig. 9. LD as a function of wavelength (left) and transmission of the sample (right). The angle of incidence to the film was 55°. Peak LD values occur from 470–490 nm, exactly near the region of most absorption.

Funding. National Science Foundation (1607358, 1918260).

Acknowledgment. The authors thank Professor Megan Paciaroni at Benedictine College in Kansas for helpful comments on this manuscript and Barry Seff at EMD Performance Materials for supplying the processing recipe of the LCP. The Plasmatherm DSE III reactive ion etcher used in this study was acquired through an NSF MRI. All SEM images and data were collected in the W. M. Keck Center for Nano-Scale Imaging in the Department of Chemistry and Biochemistry at the University of Arizona with funding from the W.M. Keck Foundation Grant.

Disclosures. Authors declare no conflicts of interest.

REFERENCES

1. R. A. Chipman, W. T. Lam, and G. Young, *Polarized Light and Optical Systems* (CRC Press, 2019).
2. V. L. Gamiz, "Performance of a four-channel polarimeter with low-light-level detection," Proc. SPIE **3121**, 35–46 (1997).

3. G. Myhre, W.-L. Hsu, A. Peinado, C. LaCasse, N. Brock, R. A. Chipman, and S. Pau, "Liquid crystal polymer full-stokes division of focal plane polarimeter," Opt. Express **20**, 27393–27409 (2012).
4. X. Tu, O. J. Spires, X. Tian, N. Brock, R. Liang, and S. Pau, "Division of amplitude RGB full-Stokes camera using micro-polarizer arrays," Opt. Express **25**, 33160–33175 (2017).
5. W.-L. Hsu, G. Myhre, K. Balakrishnan, N. Brock, M. Ibn-Elhaj, and S. Pau, "Full-Stokes imaging polarimeter using an array of elliptical polarizer," Opt. Express **22**, 3063–3074 (2014).
6. X. Zhao, A. Bermak, F. Boussaid, and V. G. Chigrinov, "Liquid-crystal micropolarimeter array for full Stokes polarization imaging in visible spectrum," Opt. Express **18**, 17776–17787 (2010).
7. J. E. Millerd and N. J. Brock, "Methods and apparatus for splitting, imaging, and measuring wavefronts in interferometry," U.S. Patent 6,552,808 (22 April 2003).
8. K. L. Marshall, K. Adelsberger, G. Myhre, and D. W. Griffin, "The LCPDI: a compact and robust phase-shifting point-diffraction interferometer based on dye-doped LC technology," Mol. Cryst. Liq. Cryst. **454**, 23/[425]–45/[447] (2006).
9. C.-T. Lee, H.-Y. Lin, and C.-H. Tsai, "Designs of broadband and wide-view patterned polarizers for stereoscopic 3D displays," Opt. Express **18**, 27079–27094 (2010).
10. C.-T. Lee and H. Y. Lin, "Ultra-wide-view patterned polarizer type stereoscopic LCDs using patterned alignment," Opt. Express **20**, 1700–1705 (2012).
11. S. Varghese, G. P. Crawford, C. W. M. Bastiaansen, D. K. G. de Boer, and D. J. Broer, "High pretilt four-domain twisted nematic liquid crystal display by microrubbing: process, characterization, and optical simulation," J. Appl. Phys. **97**, 53101 (2005).
12. R. Lu, X. Zhu, S.-T. Wu, Q. Hong, and T. X. Wu, "Ultrawide-view liquid crystal displays," J. Disp. Technol. **1**, 3–14 (2005).
13. Z. Ge, R. Lu, T. X. Wu, S.-T. Wu, C.-L. Lin, N.-C. Hsu, W.-Y. Li, and C.-K. Wei, "Extraordinarily wide-view circular polarizers for liquid crystal displays," Opt. Express **16**, 3120–3129 (2008).
14. Q. Hong, T. X. Wu, R. Lu, and S.-T. Wu, "Wide-view circular polarizer consisting of a linear polarizer and two biaxial films," Opt. Express **13**, 10777–10783 (2005).
15. Q. Hong, T. X. Wu, X. Zhu, R. Lu, and S.-T. Wu, "Designs of wide-view and broadband circular polarizers," Opt. Express **13**, 8318–8331 (2005).
16. S.-W. Oh, S.-H. Kim, J.-M. Baek, and T.-H. Yoon, "Design of an achromatic wide-view circular polarizer using normal dispersion films," J. Inf. Disp. **20**, 25–30 (2019).
17. B. Wen, M. P. Mahajan, and C. Rosenblatt, "Ultrahigh-resolution liquid crystal display with gray scale," Appl. Phys. Lett. **76**, 1240–1242 (2000).
18. T. Ishinabe, T. Miyashita, and T. Uchida, "47.2: novel wide viewing angle polarizer with high achromaticity," SID Symp. Dig. Tech. Pap. **31**, 1094–1097 (2000).
19. M. B. Ko and K. H. Park, "Polarizing plate for OLED and optical display including the same," U.S. Patent 9,563,000 (7 February 2017).
20. D. Yang and S. T. Wu, *Fundamentals of Liquid Crystal Devices* (Wiley, 2010).
21. P. Yeh and C. Gu, *Optics of Liquid Crystal Displays*, 2nd ed. (Wiley, 2010).
22. J.-W. Moon, W.-S. Kang, H. Y. Han, S. M. Kim, S. H. Lee, Y. G. Jang, C. H. Lee, and G.-D. Lee, "Wideband and wide-view circular polarizer for a transflective vertical alignment liquid crystal display," Appl. Opt. **49**, 3875–3882 (2010).
23. S.-W. Oh and T.-H. Yoon, "Achromatic wide-view circular polarizers for a high-transmittance vertically-aligned liquid crystal cell," Opt. Lett. **39**, 4683–4686 (2014).
24. G. Myhre and S. Pau, "Imaging capability of patterned liquid crystals," Appl. Opt. **48**, 6152–6158 (2009).
25. G. Myhre, A. Sayyad, and S. Pau, "Patterned color liquid crystal polymer polarizers," Opt. Express **18**, 27777–27786 (2010).
26. K. L. Marshall, G. Painter, K. Lotito, A. G. Noto, and P. Chang, "Transition metal dithiolene near-IR dyes and their applications in liquid crystal devices," Mol. Cryst. Liq. Cryst. **454**, 47/[449]–79/[481] (2006).
27. G. H. Heilmeier and L. A. Zanoni, "Guest–host interactions in nematic liquid crystals. A new electro-optic effect," Appl. Phys. Lett. **13**, 91–92 (1968).
28. S. Nersisyan, N. Tabiryan, D. M. Steeves, and B. R. Kimball, "Axial polarizers based on dichroic liquid crystals," J. Appl. Phys. **108**, 033101 (2010).
29. B.-H. Yu, J.-W. Huh, K.-H. Kim, and T.-H. Yoon, "Light shutter using dichroic-dye-doped long-pitch cholesteric liquid crystals," Opt. Express **21**, 29332–29337 (2013).
30. A. Lien, "A detailed derivation of extended Jones matrix representation for twisted nematic liquid crystal displays," Liq. Cryst. **22**, 171–175 (1997).
31. R. A. Chipman, "Mueller matrices," in *OSA Handbook of Optics* (McGraw-Hill, 1995).
32. S.-Y. Lu and R. A. Chipman, "Interpretation of Mueller matrices based on polar decomposition," J. Opt. Soc. Am. A **13**, 1106–1113 (1996).
33. Norland Products Incorporated, "Norland Optical Adhesive 73," 2020, https://www.norlandprod.com/adhesives/NOA%2073.html.
34. X. Tu, S. McEldowney, Y. Zou, M. Smith, C. Guido, N. Brock, S. Miller, L. Jiang, and S. Pau, "Division of focal plane red–green–blue full-Stokes imaging polarimeter," Appl. Opt. **59**, G33–G40 (2020).
35. W.-L. Hsu, K. Balakrishnan, M. Ibn-Elhaj, and S. Pau, "Infrared liquid crystal polymer micropolarizer," Appl. Opt. **53**, 5252–5258 (2014).